ACS OMEGA

http://pubs.acs.org/journal/acsodf

Article

An Inverse Emulsion Polymer as a Highly Effective Salt- and Calcium-Resistant Fluid Loss Reducer in Water-Based Drilling Fluids

Wenjun Shan, Jingyuan Ma, Guancheng Jiang, Jinsheng Sun, and Yuxiu An*

Cite This: *ACS Omega* 2022, 7, 16141−16151

Read Online

ACCESS | Metrics & More | Article Recommendations

ABSTRACT: To control the fluid loss of water-based drilling fluids (WBDFs) in salt-gypsum formations, a nano-SiO_2 graft copolymer was prepared by inverse emulsion polymerization. The polymer (EAANS) was prepared with acrylamide, 2-acrylamido-2-methyl-1-propane sulfonic acid, N-vinylpyrrolidone, and KH570-modified nano-silica (M-SiO_2) as raw materials. The molecular structure and morphology of EAANS were characterized by Fourier transform infrared spectroscopy, nuclear magnetic resonance, thermogravimetric analysis, transmission electron microscopy (TEM), and other methods. In the temperature range of 150 °C, 2 wt % EAANS can reduce the API filtration volume of the base slurry to within 20 mL and the HP-HT filtration volume at 150 °C to 21.8 mL. More importantly, 2 wt % EAANS can maintain the API filtration volume less than 10 mL even when the concentration of NaCl or $CaCl_2$ was as high as 36 or 30 wt %, and as the salt/calcium content increased, the amount of filtration continued to decrease. The results of TEM, X-ray diffraction, particle size distribution, and scanning electron microscopy showed that the fluid loss control mechanism of EAANS was that EAANS can form a crosslinked network structure in the solution and adsorb on the clay surface, so as to reduce the particle size of clay particles, increase the proportion of fine particles in drilling fluids, and finally form a dense filter cake to reduce the filtration volume. Because of the excellent filtration performance of EAANS at high Na^+/Ca^{2+} concentration, EAANS can become a promising WBDF fluid loss reducer in salt-gypsum formations.

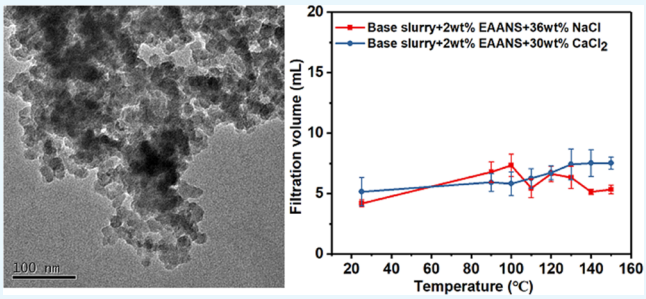

1. INTRODUCTION

A drilling fluid is one of the key technologies in the drilling process because of its functions such as balancing formation pressure, suspending and transporting cuttings, cleaning the well, and lubricating drilling tools.[1−4] Because of the low cost and low pollution to the environment, water-based drilling fluids (WBDFs) have become the main choice for oil and gas drilling.[5,6] WBDFs are usually composed of water, bentonite, tackifiers, fluid loss additives, and other functional treatment agents. During the circulation of the drilling fluid, because of the formation pressure difference, the liquid in the WBDFs will invade the formation and form a filter cake on the surface of the well wall. The liquid released by WBDFs may not only invade the formation and bring about the possibility of formation instability, but also cause changes in the performance of WBDFs and cause other downhole accidents.[7] For example, excessive filtration loss can easily lead to thickening of the mud cake, resulting in the reduction of the well diameter. In addition, the filtration volume that invades the formation easily causes the hydration of the mudstone or shale, resulting in the accident of collapsing and dropping blocks. Therefore, controlling fluid loss is crucial to maintaining the performance of WBDFs and ensuring safe drilling.

Bentonite is one of the main components that forms a suspension in WBDFs, and its stability has an important effect on maintaining the basic rheological and filtration properties of WBDFs.[8] Because of the influence of the formation conditions, bentonite particles would undergo hydration, swelling, and flocculation, resulting in the instability of bentonite suspensions.[9−13] Temperature and electrolyte ions are the most important factors that destroy the stability of bentonite particles during drilling.[12] The formation temperature increases as the drilling depth increases. Researchers have made great effort in the temperature resistance of drilling fluid treatment agents and WBDFs.[9,14−16] On the other hand, the thick salt-gypsum beds often cover abundant oil and gas resources, and the high concentration of electrolyte ions rich in the salt-gypsum beds will have a serious impact on the performance of WBDFs, among which sodium ions (Na^+,

Received: March 11, 2022
Accepted: April 13, 2022
Published: April 27, 2022

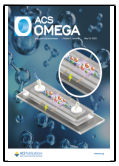

representative of monovalent ions) and calcium ions (Ca^{2+}, representative of divalent ions) are the main pollutants. Ca^{2+} pollution is particularly serious, which will cause the compression of the montmorillonite layer spacing and the flocculation of particles and seriously destroy the stability of the bentonite suspension.[17] In addition, Na^+ and Ca^{2+} may also damage the performance of WBDF treatment agents. For example, in previous studies we found that salt ions can cause changes in the conformation and morphology of polymer molecules, resulting in the deterioration of properties.[18] A recent study has shown that anhydrite (calcium sulfate) can be used as a new type of drilling fluid weighting material, thus placing great demands on the resistance of other treatments in WBDFs to Ca^{2+}.[19]

To improve the filtration performance of bentonite suspensions, various polymer-based fluid loss agents, such as xanthan gum,[20,21] starch,[22] cellulose,[8] and various synthetic polymers,[23−25] are usually added to WBDFs. Table 1 summarizes the temperature and salt resistance of polymeric fluid loss control agents used in high-temperature and high-salinity formations. Natural polymers such as xanthan gum have excellent resistance to salt/calcium pollution, but they are easily degraded when the temperature exceeds 80 °C.[26−28] Synthetic polymers can usually be used at higher temperatures but have difficulty in maintaining stability under high salt/calcium contamination.[4,29,30] Ghaderi et al. prepared a temperature- and salt-tolerant polymeric thickener that could increase the viscosity of WBDFs at salt concentrations ranging from 5000 to 50,000 ppm.[31] Hamad et al. synthesized an amphoteric polymer (PEX for short) that reduced fluid loss at high temperatures. However, the ability of PEX to reduce fluid loss under salt contamination was not investigated.[23] Although there have been studies considering the salt resistance of polymer fluid loss agents, they are mostly limited to low concentrations of salt/calcium. For example, the zwitterionic polymer PADAD maintains a filtration volume of less than 10 mL under 2 mol/L NaCl or 0.1 mol/L $CaCl_2$ contamination.[32] The quaternary copolymer (AM/AMPS/AHPS/AAc tetrapolymer) prepared by Sanam et al. can maintain low fluid loss under saturated NaCl pollution but did not investigate the performance under high-concentration Ca^{2+} pollution.[33] Similarly, the quaternary copolymers studied by Li et al. can also maintain a low filtration volume under saturated NaCl contamination,[34] but investigations on Ca^{2+} contamination are still lacking. Zhu et al. studied a polymer-grafted xanthan gum (XG-g-AAA), although it also has a certain salt tolerance, but it can only resist 0.75% $CaCl_2$ or 5% NaCl pollution after aging at 150 °C.[35] Davoodi et al. prepared polymeric treatment that can control the rheology and fluid loss of WBDFs and investigated its solubility in high-salinity water samples with varying concentrations of monovalent salts.[36] However, the fluid loss performance in high-concentration brine was not further verified. Cao et al. prepared a calcium-resistant polymer fluid loss agent (PAAV) with an anticalcium capacity of 10 wt %.[37] Liu et al. used aqueous free radical polymerization to prepare the zwitterionic polymer (ADD) as an anticalcium fluid loss agent for WBDFs, but it can only resist 11.1 wt % Ca^{2+} pollution.[38] As can be seen from Table 1, the polymer fluid loss reducers currently studied were insufficient for resisting high concentrations of Na^+ or Ca^{2+} contamination. Only a few research results were resistant to saturated NaCl. However, for $CaCl_2$, the highest level in the current study was only 11.1 wt %. One of our previous studies introduced graphene oxide into the polymer, and its calcium resistance reached 25 wt %.[39] However, at higher concentrations of calcium contamination, the polymer could not continue to maintain fluid loss reduction capacity. Thus, to reduce the fluid loss of WBDFs in the salt layer containing high concentrations of Na^+ and Ca^{2+}, it is also necessary to study the fluid loss agent with the ability to resist high salt/calcium.

Table 1. Summary of Polymer Fluid Loss Control Agents for High-Temperature and High-Salinity Formation

polymer fluid loss reducer	temperature resistance (°C)	salt resistance
xanthan gum[26−28]	below 80	excellent
PEX[23]	180	not mentioned
PADAD[32]	160	2 mol/L NaCl or 0.1 mol/L $CaCl_2$
AM/AMPS/AHPS/AAc tetrapolymer[33]	150	NaCl resistant to saturation, but no mention of $CaCl_2$
XG-g-AAA[35]	150	0.75 wt % $CaCl_2$ or 5 wt % NaCl
PAAV[37]	150	10 wt %$CaCl_2$
ADD[38]	150	11.1 wt %$CaCl_2$

The synthesis method of polymers will affect the structure, morphology, and basic properties of polymers.[18] Common polymerization methods include aqueous solution polymerization, emulsion/inverse emulsion polymerization, precipitation polymerization, and so on. Different polymerization methods affect their structure, morphology, and particle size; at the same time, these parameters control the rheological behavior of polymer fluids. We have previously prepared a nanograft copolymer by aqueous solution polymerization, which has excellent temperature resistance, but the resistance of Ca^{2+} pollution was only 2 wt %.[40] Through the research on the polymerization method, we found that the inverse emulsion polymerization method may be able to obtain polymers with higher salt/calcium resistance.[41] Therefore, in this paper, the nanografted copolymer (EAANS for short) was prepared by inverse emulsion polymerization. Through the characterization of the polymer structure and properties, we found that the polymer can effectively improve the particle size distribution (PSD) of bentonite particles under high-temperature and high salt/calcium pollution to maintain the stability of the suspension. Thus, EAANS might be suitable for controlling fluid loss during drilling in salt-gypsum formations.

2. MATERIALS AND METHODS

2.1. Materials. All materials and their functions used in this paper are shown in Table 2. Acrylamide (AM), 2-acrylamido-2-methyl-1-propane sulfonic acid (AMPS), N-vinylpyrrolidone (NVP), ammonium persulfate (APS), sodium bisulfite, paraffin liquid, nonionic surfactants Span 80, and Triton X-100 were all commercial products from Aladdin. Nano-SiO_2 which was modified by methacryloxy propyl trimethoxyl silane (KH570) was purchased from the Xianfeng Chemical Reagent Company. Isopropanol, NaOH, NaCl, $CaCl_2$, and other reagents were purchased from a domestic reagent company. Sodium bentonite was obtained from Weifang Boda company.

2.2. Synthesis of Inverse Emulsion Polymer EAANS. The nanograft copolymer EAANS was synthesized by inverse emulsion polymerization. It is consistent with the monomer ratio in our previous work.[40] The synthetic schematic diagram of EAANS is shown in Figure 1, and the specific steps were as follows: First prepare the water phase and the oil phase

https://doi.org/10.1021/acsomega.2c01476
ACS Omega 2022, 7, 16141−16151

Table 2. Materials and Their Functions Used in This Study

material	function	material	function
AM (AR)	polymerized monomer	AMPS (AR)	polymerized monomer
NVP (AR)	polymerized monomer	ammonium persulfate (APS, AR)	initiator
sodium bisulfite (AR)	initiator	paraffin liquid (AR)	oil phase solvent
Span 80 (BR)	emulsifier	Triton X-100 (BR)	emulsifier
Nano-SiO_2 (20 nm, 99%)	polymerized monomer	isopropanol (AR)	
sodium hydroxide (NaOH, AR)	pH adjuster	sodium chloride (NaCl, AR)	salt
anhydrous calcium chloride ($CaCl_2$, AR)	salt	sodium bentonite	pulping soil

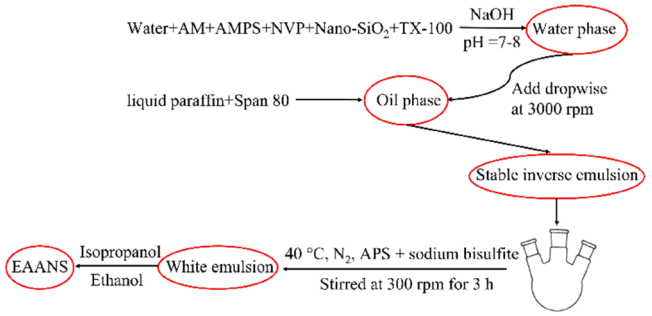

Figure 1. Synthesizing scheme of EAANS.

separately: AM, AMPS, nano-SiO_2, NVP, and TX-100 were dissolved in deionized water to obtain the water phase, and NaOH was used to adjust the pH of the solution to 7−8. The emulsifier Span 80 was dissolved in liquid paraffin to obtain the oil phase. Then, the water phase was added dropwise to the oil phase under the stirring of a high-speed shear emulsification mixer (JRJ300-D1, China) at 3000 rpm, and the mixture was stirred for 30 min to form a stable inverse emulsion. Then, the inversed emulsion was transferred to a three-necked reaction flask and placed in a water bath at 40 °C and continued to stir at 300 rpm under the protection of nitrogen. After 30 min, APS and sodium bisulfite were added to initiate polymerization. After continuing the reaction for 3 h, the obtained white emulsion was precipitated with isopropanol, and after repeated washing with ethanol several times, the product was dried at 60 °C and pulverized to obtain EAANS.

2.3. Characterization of EAANS. Fourier transform infrared spectroscopy (FT-IR, Horiba, Germany) of EAANS was performed with a resolution of 4 cm^{-1} and a wavenumber range of 4000−600 cm^{-1}.About 5 mg of EAANS was dissolved in 0.5 mL of deuterated chloroform ($CDCl_3$) for 1H nuclear magnetic resonance spectral analysis (^{1}H NMR, JEOL, Japan). The synchronous thermal analyzer TGA/DSC 1 (METTLER TOLEDO) was used to investigate the thermal stability of EAANS at 30−600 °C. The test was carried out in a nitrogen environment with a heating rate of 10 °C/min. EAANS were dissolved in deionized water and dropped onto amorphous carbon-coated copper grids for transmission electron microscope (TEM, JEM2010, JEOL, Japan) and scanning electron microscope (SEM, JSM7401, JEOL, Japan) observations. The powdered polymer was observed by SEM and tested for PSD (Nano ZS90, Malvern Instrument, UK).

2.4. Preparation of the Base Slurry. For the preparation of the base slurry and drilling fluid, refer to Drilling Fluid Technology[42] published by China University of Petroleum Press and API standards formulated by American Petroleum Institute. The prehydrated bentonite base slurry was prepared by mixing 40 g of bentonite and 2.5 g of anhydrous sodium carbonate in 1000 mL of water and continuously stirring at 800 rpm for 16 h. In this work, the prehydrated bentonite base slurry was used to directly evaluate the fluid loss reduction capability of EAANS without the addition of other drilling fluid treatments. The base slurry has a density of 1.05 g/cm^3 and a pH value of around 8. A certain concentration of EAANS was slowly added to the base slurry at a stirring speed of 8000 rpm, and stirring was continued for 10 min. After that, different concentrations of NaCl or $CaCl_2$ were added to simulate the pollution of different salts in the formation.

2.5. Performance Evaluation. The API filtration volume of the drilling fluid was tested using medium-pressure filtration apparatus (MOD.SD3, China) according to API standards. The drilling fluid was poured into an aging tank and hot-rolled at a specified temperature (90, 120, and 150 °C) in a high-temperature roller heating furnace (XGRL-4A, China). The rolling time was fixed at 16 h. API filtration tests were performed before and after the thermal aging experiments. In addition, high-pressure and high-temperature (HP-HT) filtration was also carried out at a pressure difference of 3.5 MPa and a temperature of 150 °C. A six-speed rotational viscometer (ZNN-D6S, China) was used to test the rheology of the fluid. The rheological parameters such as apparent viscosity (AV), plastic viscosity (PV), and yield point (YP) were calculated from the value of Ø600 (reading of 600 rpm) and Ø300 (reading of 300 rpm) using the following formulas:

$$\mathrm{AV} = 0.5\ \text{Ø600}\ (\mathrm{mPa{\cdot}s}) \quad (1)$$

$$\mathrm{PV} = \text{Ø600} - \text{Ø300}\ (\mathrm{mPa{\cdot}s}) \quad (2)$$

$$\mathrm{YP} = (2\ \text{Ø300} - \text{Ø600})/2\ (\mathrm{Pa}) \quad (3)$$

2.6. Mechanism Analysis. X-ray diffraction (XRD), PSD, and SEM were used to analyze the fluid loss control mechanism of EAANS. The base slurry and base slurry containing 2 wt % EAANS or different salts were prepared and aged at different temperatures. A portion of the liquid was taken directly for PSD (Bettersize 2000, China), the remaining liquid was dried at 60 °C and ground into powder, and then XRD testing was performed using a D8 ADVANCE (Bruker, Germany). Images were collected between 5 and 80° in 0.02° steps at a scan speed of 4°/min. The layer spacing of clay (d_{001}) was analyzed using Bragg's equation. The value for $n = 1$ was calculated for $2d \sin 2\theta = n\lambda$ ($\lambda = 0.15406$ nm). The microscopic morphology of the filter cake was observed by SEM (JSM7401, JEOL, Japan). The filter cakes obtained from the fluid loss experiment were first rinsed with deionized water to remove the floating false filter cake. Then, the filter cakes were dried at 60 °C for 24 h and then cut up into squares of sizes 0.5 cm^2 × 0.5 cm^2. The dried and cut samples were adhered to conductive tapes and then metal-sprayed for 2 min.

3. RESULTS AND DISCUSSION

3.1. Characterization. The chemical structure of EAANS was clarified by FT-IR and ^{1}H NMR. The FT-IR spectrum of EAANS is shown in Figure 2a. The characteristic absorption peaks of free amine groups and associated amine groups

https://doi.org/10.1021/acsomega.2c01476
ACS Omega 2022, 7, 16141−16151

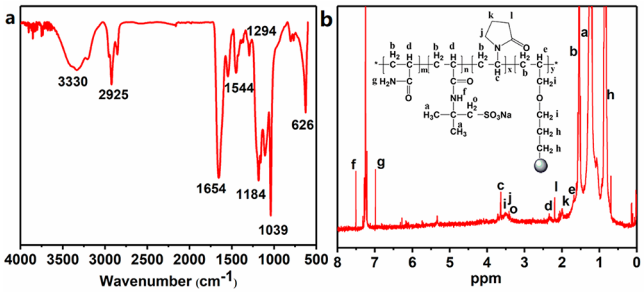

Figure 2. (a) FT-IR and (b) ^{1}H NMR of EAANS.

($-NH_2$) were at 3330 cm^{-1}; those at 1650, 1544, and 1294 cm^{-1} were attributed to amide I (C═O), amide II (C−N), and amide III, respectively. The characteristic absorption peak of methylene ($-CH_2$) was 2925 cm^{-1}, and the asymmetric tensile and flexural vibration peaks of Si-O-Si were at 1184, 1039, and 626 cm^{-1}. The characteristic peaks of AM, AMPS, NVP, and nano-SiO_2 all appeared in the FT-IR spectrum of EAANS, indicating the successful preparation of EAANS. On the other hand, the ^{1}H NMR of EAANS is shown in Figure 2b, and the methylene protons ($-CH_2-$) and methine protons (−CH−) in the polymer backbone appear at 1.4−1.6 and 1.9−2.4 ppm, respectively. The methyl proton and methylene proton ($-CH_2-$ of $-CH_2SO_3-$) in AMPS correspond to 1.0−1.4 and 3.0−3.4 ppm, respectively. The amino protons (−NH−) in AM and AMPS appear at 7.0−8.0 ppm. The three different protons of the pyridyl unit in NVP appear at 1.98, 2.19, and 3.39 ppm, respectively. In addition, the two methylene protons ($-CH_2-$) in the nano-SiO_2 modified by KH570 appeared at 0.7−1.0 and 3.4−3.5 ppm. Therefore, the results of ^{1}H NMR showed that the characteristic structures of AM, AMPS, NVP, and nano-SiO_2 all appeared in the structure of EAANS.

Thermogravimetric analysis (TGA) was performed on EAANS in an N_2 atmosphere to characterize its thermal stability. As shown in Figure 3, according to the downward

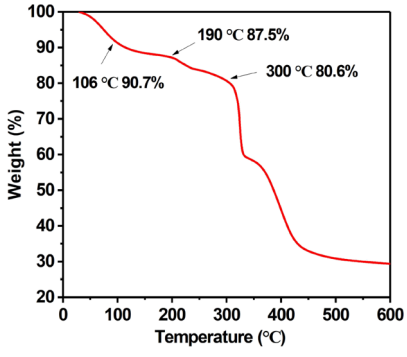

Figure 3. TGA curves of EAANS.

trend of the TGA curve, the weight loss of EAANS was divided into three stages: from 30 to 106 °C, the weight loss of EAANS was about 10%, which was caused by the evaporation of the bound water in the polymer. The weight loss of EAANS was about 10% between 106 and 300 °C, which was related to the decomposition of the amide group in the polymer side chain. Finally, when the temperature exceeded 300 °C, EAANS lost weight rapidly, which might be related to the breaking of the sulfonic acid groups and C−C bonds in the polymer chain. The results of TGA showed that EAANS can maintain the stability of the polymer structure within 200 °C.

The microscopic morphology of EAANS was observed by TEM and SEM. As shown in Figure 4a, EAANS in the aqueous solution has an obvious tendency to agglomerate. After increasing the magnification, it can be seen that EAANS has a circular structure similar to nano-SiO_2. The size of the agglomerated EAANS shown in Figure 4a1 was about 2 μm, which was consistent with the PSD results of EAANS in Figure 4c, and its particle size was mainly distributed in 1000−4000 nm range. Figure 4b showed the solid state of EAANS after drying. It can be seen from the SEM image that the solid particles of EAANS presented a large number of pore-like structures. The porous structure makes EAANS have a large specific surface area, which can increase the dissolution rate of EAANS in the solution.

3.2. Fluid Loss Performance of EAANS in WBDFs.

Keeping low fluid loss is an important indicator of drilling fluids. API standards stipulate that fluid loss should not exceed 20 mL within 30 min.[43] Figure 5a showed the filtration volumes of the base slurry with different concentrations of EAANS before and after aging at 150 °C. Clearly, the filtration volume of the slurry continued to decrease with the increase of EAANS concentration. When the concentration of EAANS exceeded 1.5 wt %, the filtration volume of the slurry can be kept within 20 mL both before and after aging. Therefore, the concentration of EAANS was immobilized to 2 wt % in subsequent experiments. The influence of EAANS on the filtration property of the base slurry at different temperatures is shown in Figure 5b. The base slurry has a high filtration volume (34.6 mL) at room temperature. As the aging temperature increased, the filtration volume of the base slurry continued to rise. When the temperature exceeded 140 °C, the increase rate of the filtration volume of the base slurry became faster. The filtration volume of the base slurry was significantly reduced after EAANS was added; 2 wt % of EAANS reduced the filtration volume of the base slurry to 8.6 mL at room temperature. After that, as the aging temperature increased, the filtration volume of the base slurry containing 2 wt % EAANS slowly increased, and the filtration volume of the system can always be less than 20 mL within the range of 150 °C. To further verify the fluid loss reduction ability of EAANS at high temperature, the HP-HT filtration volume of the base slurry and the base slurry containing 2 wt % EAANS at 150 °C was tested, and the results are shown in Table 3. Obviously, EAANS effectively reduced the HP-HT filtration volume of the base slurry. Both the API medium pressure fluid loss test and HP-HT test results showed that EAANS can effectively reduce the filtration volume of drilling fluids within 150 °C, and EAANS can be a potential fluid loss reducer for drilling fluids.

Na^+ and Ca^{2+} are usually used to represent the salt ions in the formation. The ability of EAANS to resist salt/calcium pollution was evaluated by gradually adding different concentrations of NaCl and $CaCl_2$ to the base slurry containing 2 wt % EAANS. The tolerance of EAANS to different concentrations of NaCl and $CaCl_2$ at different temperatures is shown in Figure 6. The filtration volume of the base slurry containing 2 wt % EAANS before aging and after aging at 90, 120, and 150 °C was 8.6, 11.1, 14.5, and 16.7 mL, respectively. After adding 5 wt % NaCl, except before aging, the filtration volume of the slurry after aging at any temperature would increase. However, as the concentration of NaCl continued to increase, the filtration volume began to

https://doi.org/10.1021/acsomega.2c01476
ACS Omega 2022, 7, 16141−16151

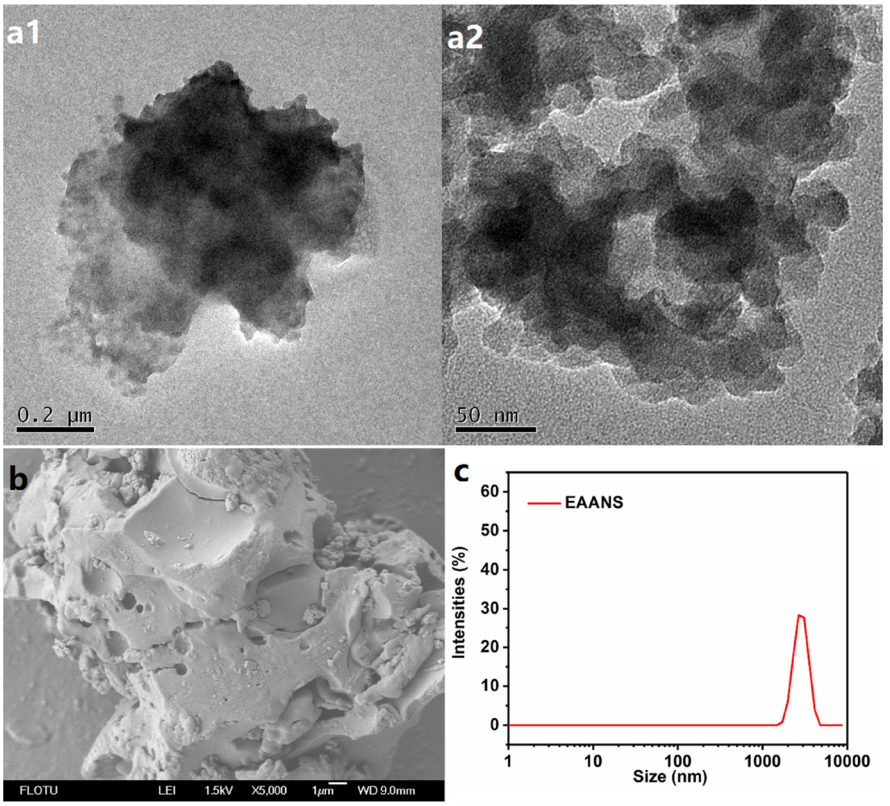

Figure 4. Microstructure of EAANS. (a) TEM; (b) SEM; (c) PSD.

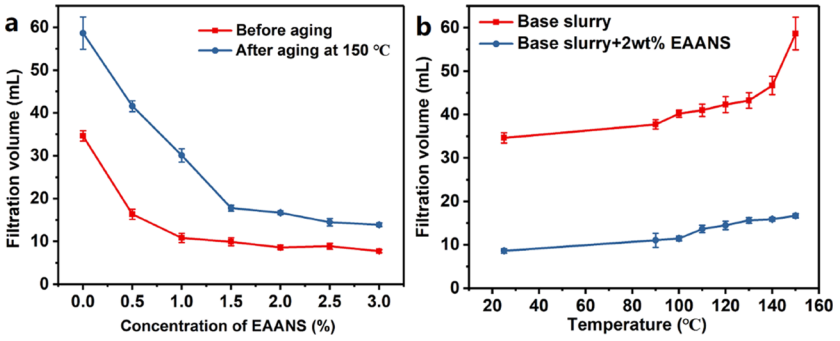

Figure 5. (a) Filtration volume of the base slurry with different concentrations of EAANS; (b) filtration volume of the base slurry with or without EAANS at different temperatures.

Table 3. HP-HT Filtration Volume of the Base Slurry and Base Slurry Containing 2 wt % EAANS after Aging at 150 °C

temperature	fluid	HP-HT filtration volume (mL)
150 °C	base slurry	all lost
	base slurry containing 2 wt % EAANS	21.8

decrease. At low temperatures (<120 °C), 2 wt % EAANS always maintained a filtration volume of less than 20 mL within the NaCl concentration range of 0−36 wt %. As the temperature reached 150 °C, only the NaCl concentration reached 15% can 2 wt % EAANS maintain a low filtration volume. Therefore, from the results of Figure 6a, it can be seen that EAANS can exhibit a better fluid loss reduction ability than low NaCl concentration under high NaCl contamination. Contrary to NaCl, EAANS always maintains strong resistance to $CaCl_2$ pollution (Figure 6b). Within 150 °C, even if the concentration of $CaCl_2$ increased to 30 wt %, the base slurry containing 2 wt % EAANS can always maintain a filtration volume below 9 mL, and as the concentration of $CaCl_2$ increased, the filtration volume continued to decrease.

To further evaluate the ability of EAANS to resist high salt/calcium pollution, the filtration volume of the base slurry containing 2 wt % EAANS under high salt/calcium concentration in a temperature range of 150 °C was tested. The results are shown in Figure 7. Within the temperature range of 150 °C, the filtration volume of the base slurry containing 2 wt % EAANS was always less than 10 mL, regardless of the pollution of 36 wt % NaCl or 30 wt % $CaCl_2$, indicating that EAANS can always maintain a low filtration volume in high salt or calcium formations.

3.3. Rheological Properties of EAANS in WBDFs. Figure 8 showed the rheological changes of the base slurry after adding 2 wt % EAANS. Because our base slurry contains only

https://doi.org/10.1021/acsomega.2c01476
ACS Omega 2022, 7, 16141−16151

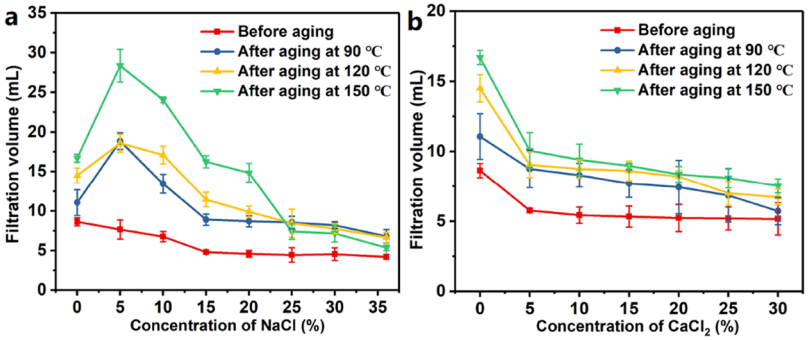

Figure 6. Filtration volume of the base slurry containing 2 wt % EAANS at different (a) NaCl or (b) $CaCl_2$ concentrations.

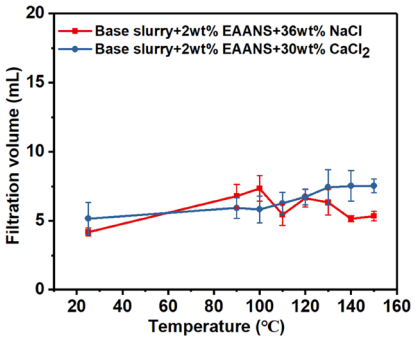

Figure 7. Filtration volume of the base slurry containing 2 wt % EAANS under high salt concentration at different temperatures.

sodium bentonite and no other treatment agents such as tackifiers are added, the viscosity of the base slurry was extremely low, and the change with temperature was also small. The AV of the base slurry after aging at a temperature below 150 °C was always lower than 5 mPa·s, while the AV of the fluid increased significantly after adding EAANS. With the increase of the aging temperature, the AV gradually increased until after aging at 130 °C, the AV decreased slightly, but was still higher than 30 mPa·s. This showed that EAANS can effectively increase the viscosity of the fluid, which was more conducive to suspending cuttings.[44] On the other hand, the YP of the drilling fluid measures the ability of the fluid to carry cuttings. Larger YP can carry coarse-grained cuttings under a smaller annulus upward velocity.[45−48] It can be seen from Figure 8b that with the increase of aging temperature, EAANS can significantly improve the YP of the fluid. That is, EAANS can improve the rock-carrying ability of fluids.

3.4. Mechanism Analysis of Fluid Loss Control. The microscopic morphology of the aged EAANS was shown in the TEM image in Figure 9. EAANS in solution became different after aging than before aging, and linear molecular chains of EAANS can be seen in Figure 8, which were crosslinked with each other. The stretched polymer molecular chain is more conducive to the exposure of functional groups on the polymer, thereby enhancing the interaction with the clay particles. The crosslinked molecular chains further increase the viscosity of the fluid. According to Darcy's law of permeability, the filtration rate (dVf/dt, cm^3/s) equation of the drilling fluid can be derived: $dVf/dt = KA\Delta p/\mu h$, where K is the permeability of the filter cake, A is the area of the cake (cm^3), μ is the viscosity of the filtrate, h is the thickness of the cake, and Δp is the pressure drop (0.69 MPa). It can be seen that the higher the viscosity of the fluid, the more favorable it is to reduce the filtration rate.

The change of the clay layer spacing (d_{001}) can be analyzed by XRD. As shown in Figure 10, the d_{001} of fully hydrated bentonite in the base slurry after losing free water was 1.208 nm. After adding EAANS, the d_{001} of bentonite/EAANS decreased to 0.991 nm. The decrease of d_{001} indicated that the clay layer spacing was compressed, which was caused by the adsorption of EAANS on the clay surface. After aging at 120 °C, the d_{001} of bentonite/EAANS was 0.987 nm, and there was no significant change, indicating that the aging process did not affect the adsorption of EAANS on the surface of bentonite.

The PSD of bentonite particles directly affects the accumulation of particles in the fluid loss process, thereby affecting the quality of the filter cake. Therefore, the fluid loss reduction mechanism of EAANS was analyzed by the PSD test of bentonite particles in the slurry. D_{10}, D_{50}, and D_{90} indicate the particle size when the cumulative particle size reaches 10, 50, and 90%, respectively. The average particle size is usually represented by D_{50}. As shown in Figure 11, after aging at 120 °C, the PSD of the base slurry was relatively concentrated, with

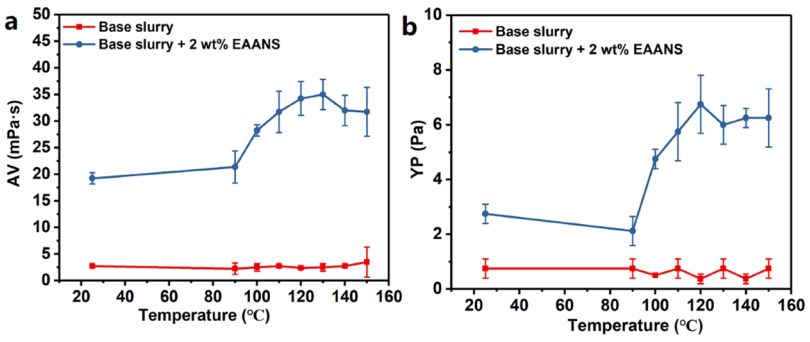

Figure 8. Rheology of the base slurry and base slurry containing 2 wt % EAANS after aging at different temperatures. (a) AV; (b) YP.

https://doi.org/10.1021/acsomega.2c01476
ACS Omega 2022, 7, 16141−16151

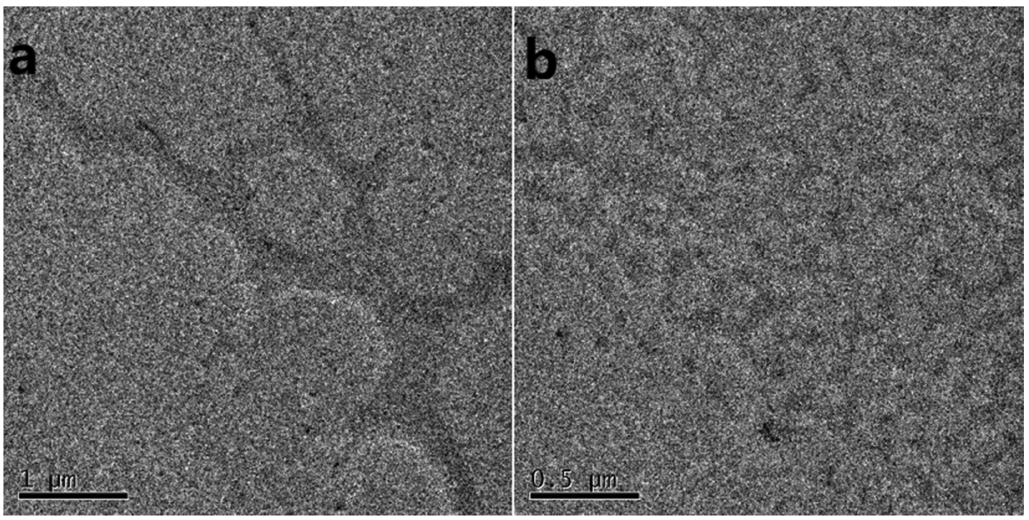

Figure 9. TEM images of EAANS after aging at 120 °C. (a) Resolution is 1 μm; (b) resolution is 0.5 μm.

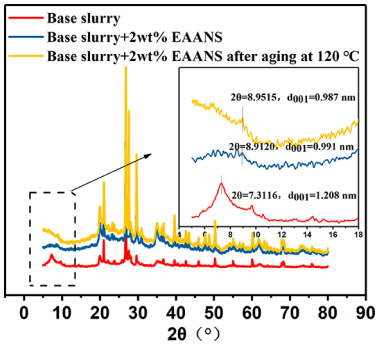

Figure 10. XRD patterns of the base slurry and base slurry containing 2 wt % EAANS.

a D_{50} of 39.38 μm. However, after adding 2 wt % EAANS, the particle size of the slurry was significantly reduced, the D_{50} was reduced to 2.33 μm, and the PSD became wider. The increase of fine particles and a wider range of PSD help to form a denser filter cake, because they can block smaller pores, thereby reducing the permeability of the filter cake.

The PSD curves of the base slurry containing 2 wt % EAANS after aging at different temperatures are shown in Figure 12. The PSD of the base slurry containing 2 wt % EAANS had similar characteristics at different temperatures, including a region less than 0.1 μm and a region of 1−10 μm. It can also be seen from Table 4 that as the temperature increased, the D_{10}, D_{50}, and D_{90} of the base slurry containing 2 wt % EAANS were very close, and the average particle size D_{50} showed a slow decrease trend. Interestingly, it can be seen from Figure 12 that as the temperature increases, the content of small particles in the system increases significantly. At 100 °C, the content of fine particles below 0.1 μm was only 6.3%, and as the temperature increased, its content gradually increased to 20.8, 19.8, 38.8, 36.1, and 78.2%. That is, after aging at 150 °C, about 80% of the particles in the slurry were at the nanometer level. However, the pore size of API standard filter paper is at the micron level.[49] Before the filter cake was formed, the nanometer-level fine particles cannot stay on the surface of the filter paper. This explained the reason why the slurry filtration volume increased gradually with the increase of temperature.

In the presence of 36 wt % NaCl or 30 wt % $CaCl_2$, the PSD curves of the base slurry and the base slurry containing 2 wt % EAANS are shown in Figure 13. After adding 36 wt % NaCl or 30 wt % $CaCl_2$ to the base slurry, the D_{50} of the particles increased from 39.38 to 97.22 or 303.2 μm, respectively (Table 5). The increase in D_{50} was due to the compressive effect of excessive Na^+ and divalent Ca^{2+} on the diffusive electric double layer of clay particles, which results in a thinning of the clay hydration layer and flocculation and a significant increase in filtration volume. Interestingly, in the presence of EAANS, the particle size of the clay particles was no longer affected by Na^+ or Ca^{2+}. WBDFs containing EAANS can still maintain a low

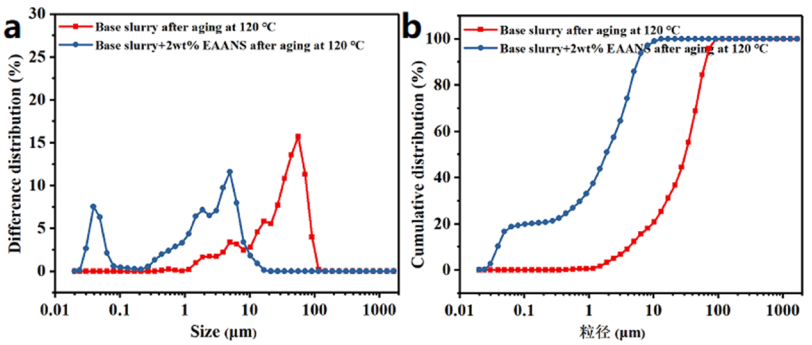

Figure 11. PSD curves of the base slurry with or without 2 wt % EAANS after aging at 120 °C. (a) Difference distribution; (b) cumulative distribution.

https://doi.org/10.1021/acsomega.2c01476
ACS Omega 2022, 7, 16141−16151

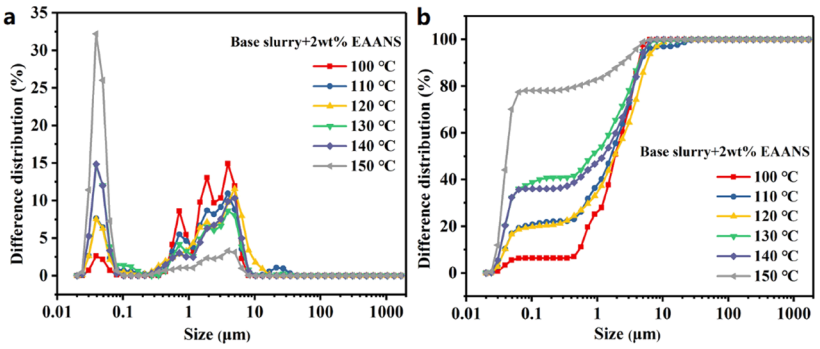

Figure 12. PSD curves of the base slurry containing 2 wt % EAANS after aging at different temperatures. (a) Difference distribution; (b) cumulative distribution.

Table 4. PSD of the Base Slurry Containing 2 wt % EAANS after Aging at Different Temperatures

	particle size distribution (μm)		
temperatures (°C)	D_{10}	D_{50}	D_{90}
100	0.685	2.366	5.341
110	0.049	2.059	5.820
120	0.049	2.330	7.062
130	0.042	1.021	5.440
140	0.042	1.566	5.677
150	0.038	0.051	3.054

particle size and a wider PSD. This was because EAANS was tightly adsorbed on the surface of the clay particles, thus avoiding the intrusion of Na^+ or Ca^{2+} into the clay layers. Therefore, a dense filter cake can still be formed to keep the filtration volume low.

The removal of the filter cake is a big issue in the petroleum industry, and there have been many studies discussing filter cake removal methods.[50−53] The thickness, smoothness, and compactness of the filter cake have important influence on the drilling process. Generally, the filter cake of the drilling fluid is required to have low thickness, high lubricity, and compactness. The photographs and SEM images of the fresh filter cake confirmed the ability of EAANS to form a dense filter cake. Figure 14 showed the filter cake formed by the base slurry containing 2 wt % EAANS and slurry containing 36 wt % NaCl or 30 wt % $CaCl_2$ after aging at 120 °C. The filter cakes containing EAANS were all very thin. From the SEM image, it can be seen that the filter cakes were very dense without obvious pores. The microscopic morphology of the filter cake containing $CaCl_2$ was different, and there were a lot of flaky structures on the surface of the filter cake, which might be caused by $CaCl_2$. The flaky particles were randomly inserted upright or obliquely on the surface of the filter cake and connected to each other. The pores formed by the accumulation of flake particles can be seen on the surface of the filter cake, but because of the layered accumulation of the flake structure, the inside of the filter cake was still very dense, and a low filtration volume can still be obtained.

The mechanism of EAANS reducing fluid loss is shown in Figure 15. The polymer chain of EAANS has a large number of polar groups such as amino groups ($-NH_2$) and sulfonic acid groups ($-SO_3^-$), which can form hydrogen bond between molecules, and the polymer chains are crosslinked to each other to form a network structure. The exposed oxygen atoms on the surface of bentonite can form hydrogen bonds with the polar groups on the EAANS, so that the EAANS is tightly adsorbed on the surface of the clay particles, which is conducive to the accumulation of particles in the process of filter cake formation and finally forms a dense filter cake and reduces the filtration loss.

4. CONCLUSIONS

The grafted copolymer EAANS of AM, AMPS, NVP, and nano-SiO_2 was prepared by inverse emulsion polymerization. EAANS was characterized by FT-IR, ^{1}H NMR, TGA, TEM, SEM, and particle size analysis. The fluid loss control mechanism of EAANS was also analyzed by TEM, XRD, PSD, and SEM. EAANS has a porous structure, which can be quickly dissolved in aqueous solution, shortening the preparation time of the drilling fluid. The specific conclusions are as follows:

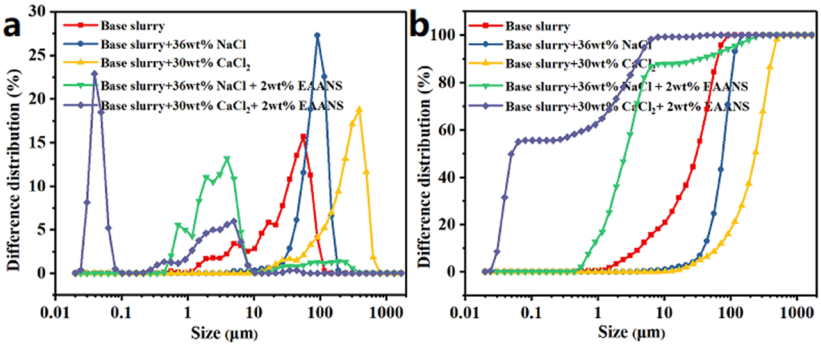

Figure 13. PSD curves of the base slurry containing NaCl or $CaCl_2$ after aging at 120 °C. (a) Difference distribution; (b) cumulative distribution.

https://doi.org/10.1021/acsomega.2c01476
ACS Omega 2022, 7, 16141−16151

Table 5. PSD of the Base Slurry Containing NaCl or $CaCl_2$ after Aging at 120 °C

drilling fluid	particle size distribution (μm)		
	D_{10}	D_{50}	D_{90}
base slurry	5.393	39.380	78.800
base slurry +36 wt % NaCl	50.960	97.220	140.600
base slurry +30 wt % $CaCl_2$	80.590	303.200	522.300
base slurry +36 wt % NaCl +2 wt % EAANS	1.011	3.303	43.220
base slurry +30 wt % $CaCl_2$+ 2 wt % EAANS	0.039	0.063	5.245

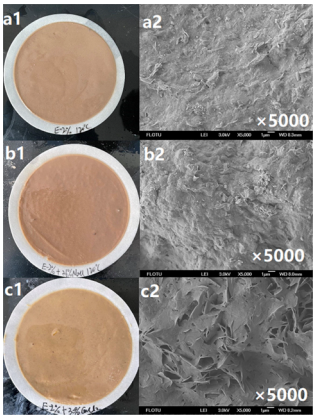

Figure 14. (1) Photograph and (2) SEM image of the filter cakes. (a) Base slurry containing 2 wt % EAANS. (b) Base slurry containing 2 wt % EAANS and 36 wt % NaCl. (c) Base slurry containing 2 wt % EAANS and 30 wt % $CaCl_2$.

(1) Filtration experiments showed that, in the temperature range of 150 °C, EAANS could reduce the API filtration volume of the base slurry to less than 20 mL, while the HP-HT filtration volume at 150 °C was only 21.8 mL.

(2) EAANS can maintain a low filtration volume under the pollution of 15−36 wt % NaCl or 0−30 wt % $CaCl_2$. More importantly, as the salt/calcium content increased, the filtration volume continued to decrease.

(3) The crosslinked network structure of EAANS in solution makes it closely adsorbed on the surface of clay particles, so as to optimize the PSD range of clay particles, which is conducive to the accumulation of particles in the process of filter cake formation and finally forms a dense filter cake and reduces the filtration loss. Even under high Na^+/Ca^{2+} contamination, EAANS can still maintain the adsorption of clay particles and improve the PSD in the slurry.

(4) Because of the excellent filtration performance of EAANS at high Na^+/Ca^{2+} concentration, EAANS can become a promising WBDF fluid loss reducer in salt-gypsum formations at temperatures below 150 °C.

AUTHOR INFORMATION

Corresponding Author

Yuxiu An − *School of Engineering and Technology, China University of Geosciences (Beijing), Beijing 100083, China; Key Laboratory of Deep Geo Drilling Technology, Ministry of Land and Resources, Beijing 100083, China;* orcid.org/0000-0002-3156-0655; Email: anyx@cugb.edu.cn, 13522045597@163.com

Authors

Wenjun Shan − *School of Petroleum Engineering, China University of Petroleum (Beijing), Beijing 102249, China; Oil & Gas Survey, China Geological Survey, Beijing 100083, China*

Jingyuan Ma − *School of Engineering and Technology, China University of Geosciences (Beijing), Beijing 100083, China; Key Laboratory of Deep Geo Drilling Technology, Ministry of Land and Resources, Beijing 100083, China*

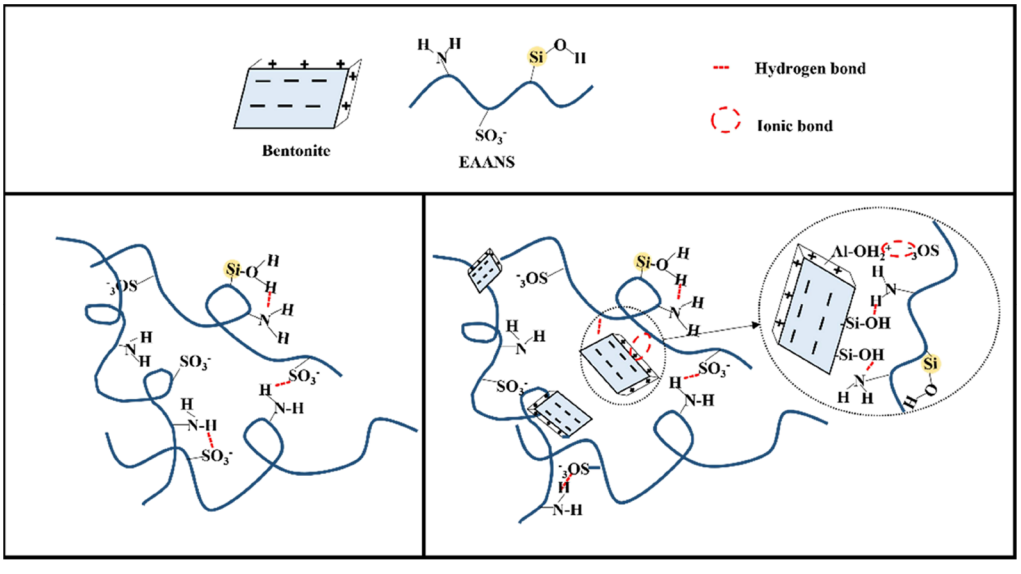

Figure 15. Schematic diagram of the mechanism of EAANS reducing fluid loss.

https://doi.org/10.1021/acsomega.2c01476
ACS Omega 2022, 7, 16141−16151

Guancheng Jiang − *School of Petroleum Engineering, China University of Petroleum (Beijing), Beijing 102249, China*
Jinsheng Sun − *School of Petroleum Engineering, China University of Petroleum (East China), Qingdao, Shandong Province 266580, China*

Complete contact information is available at: https://pubs.acs.org/10.1021/acsomega.2c01476

Notes

The authors declare no competing financial interest.

■ ACKNOWLEDGMENTS

We would like to acknowledge the financial support from the National Natural Science Foundation of China (41802196), the National Key R&D Program of China (2016YFE0202200), and the Basic Research Program on Deep Petroleum Resource Accumulation and Key Engineering Technologies (U19B6003) for support of this work.

■ REFERENCES

(1) Saboori, R.; Sabbaghi, S.; Kalantariasl, A. Improvement of rheological, filtration and thermal conductivity of bentonite drilling fluid using copper oxide/polyacrylamide nanocomposite. *Powder Technol.* **2019**, *353*, 257−266.
(2) Zhang, X.; Jiang, G.; Xuan, Y.; Wang, L.; Huang, X. Associating Copolymer Acrylamide/Diallyldimethylammonium Chloride/Butyl Acrylate/2-Acrylamido-2-methylpropanesulfonic Acid as a Tackifier in Clay-Free and Water-Based Drilling Fluids. *Energy Fuels* **2017**, *31*, 4655−4662.
(3) Ferreira, C. C.; Teixeira, G. T.; Lachter, E. R.; Veiga Nascimento, R. S. Partially hydrophobized hyperbranched polyglycerols as non-ionic reactive shale inhibitors for water-based drilling fluids. *Appl. Clay Sci.* **2016**, *132*−*133*, 122−132.
(4) Al-Hameedi, A. T. T.; Alkinani, H. H.; Dunn-Norman, S.; Al-Alwani, M. A.; Alshammari, A. F.; Albazzaz, H. W.; Alkhamis, M. M.; Alashwak, N. F.; Mutar, R. A. Insights into the application of new eco-friendly drilling fluid additive to improve the fluid properties in water-based drilling fluid systems. *J. Pet. Sci. Eng.* **2019**, *183*, No. 106424.
(5) Huang, D.; Xie, G.; Luo, P.; Deng, M.; Wang, J. Synthesis and mechanism research of a new low molecular weight shale inhibitor on swelling of sodium montmorillonite. *Energy Sci. Eng.* **2020**, *8*, 1501−1509.
(6) An, Y.; Jiang, G.; Ren, Y.; Zhang, L.; Qi, Y.; Ge, Q. An environmental friendly and biodegradable shale inhibitor based on chitosan quaternary ammonium salt. *J. Pet. Sci. Eng.* **2015**, *135*, 253−260.
(7) Jiang, G.; Sun, J.; He, Y.; Cui, K.; Dong, T.; Yang, L.; Yang, X.; Wang, X. Novel water-based drilling and completion fluid technology to improve wellbore quality during drilling and protect unconventional reservoirs. *Engineering* **2021**, DOI: 10.1016/j.eng.2021.11.014.
(8) Li, M.-C.; Wu, Q.; Song, K.; Qing, Y.; Wu, Y. Cellulose Nanoparticles as Modifiers for Rheology and Fluid Loss in Bentonite Water-based Fluids. *ACS Appl. Mater. Interfaces* **2015**, *7*, 5006−5016.
(9) Xiong, Z.-Q.; Li, X.-D.; Fu, F.; Li, Y.-N. Performance evaluation of laponite as a mud-making material for drilling fluids. *Pet. Sci.* **2019**, *16*, 890−900.
(10) Choo, K. Y.; Bai, K. Effects of bentonite concentration and solution pH on the rheological properties and long-term stabilities of bentonite suspensions. *Appl. Clay Sci.* **2015**, *108*, 182−190.
(11) Hammadi, L.; Boudjenane, N.; Belhadri, M. Effect of polyethylene oxide (PEO) and shear rate on rheological properties of bentonite clay. *Appl. Clay Sci.* **2014**, *99*, 306−311.
(12) Ben Azouz, K.; Bekkour, K.; Dupuis, D. Influence of the temperature on the rheological properties of bentonite suspensions in aqueous polymer solutions. *Appl. Clay Sci.* **2016**, *123*, 92−98.
(13) Magzoub, M. I.; Nasser, M. S.; Hussein, I. A.; Benamor, A.; Onaizi, S. A.; Sultan, A. S.; Mahmoud, M. A. Effects of sodium carbonate addition, heat and agitation on swelling and rheological behavior of Ca-bentonite colloidal dispersions. *Appl. Clay Sci.* **2017**, *147*, 176−183.
(14) Huang, X.; Lv, K.; Sun, J.; Lu, Z.; Bai, Y.; Shen, H.; Wang, J. Enhancement of thermal stability of drilling fluid using laponite nanoparticles under extreme temperature conditions. *Mater. Lett.* **2019**, *248*, 146−149.
(15) Kosynkin, D. V.; Ceriotti, G.; Wilson, K. C.; Lomeda, J. R.; Scorsone, J. T.; Patel, A. D.; Friedheim, J. E.; Tour, J. M. Graphene Oxide as a High-Performance Fluid-Loss-Control Additive in Water-Based Drilling Fluids. *ACS Appl. Mater. Interfaces* **2012**, *4*, 222−227.
(16) Akpan, E. U.; Enyi, G. C.; Nasr, G.; Yahaya, A. A.; Ahmadu, A. A.; Saidu, B. Water-based drilling fluids for high-temperature applications and water-sensitive and dispersible shale formations. *J. Pet. Sci. Eng.* **2019**, *175*, 1028−1038.
(17) Lin, L.; Luo, P. Effect of polyampholyte-bentonite interactions on the properties of saltwater mud. *Appl. Clay Sci.* **2018**, *163*, 10−19.
(18) Ma, J.; Yu, P.; Xia, B.; An, Y. Effect of salt and temperature on molecular aggregation behavior of acrylamide polymer. *E-Polymers* **2019**, *19*, 594−606.
(19) Murtaza, M.; Tariq, Z.; Mahmoud, M.; Kamal, M. S.; Al-Shehri, D. Anhydrite (Calcium Sulfate) Mineral as a Novel Weighting Material in Drilling Fluids. *J. Energy Res. Technol.* **2020**, *143*, No. 023002.
(20) Nee, L. S.; Jan, B. M.; Ali, B. S.; Mohd, N. I. The Effects of Glass Bubbles, Clay, Xanthan Gum and Starch Concentrations on the Density of Lightweight Biopolymer Drilling Fluid. *Appl. Mech. Mater.* **2014**, *625*, 526−529.
(21) Navarrete, R. C., Himes, R. E., Seheult, J. M. Applications of Xanthan Gum in Fluid-Loss Control and Related Formation Damage. In *SPE Permian Basin Oil and Gas Recovery Conference*; Society of Petroleum Engineers: Midland, Texas, 2000, p. 21.
(22) Nasiri, A.; Ameri Shahrabi, M. J.; Sharif Nik, M. A.; Heidari, H.; Valizadeh, M. Influence of monoethanolamine on thermal stability of starch in water based drilling fluid system. *Pet. Explor. Dev.* **2018**, *45*, 167−171.
(23) Hamad, B. A.; He, M.; Xu, M.; Liu, W.; Mpelwa, M.; Tang, S.; Jin, L.; Song, J. A Novel Amphoteric Polymer as a Rheology Enhancer and Fluid-Loss Control Agent for Water-Based Drilling Muds at Elevated Temperatures. *ACS Omega* **2020**, *5*, 8483−8495.
(24) Mao, H.; Qiu, Z.; Shen, Z.; Huang, W. Hydrophobic associated polymer based silica nanoparticles composite with core-shell structure as a filtrate reducer for drilling fluid at utra-high temperature. *J. Pet. Sci. Eng.* **2015**, *129*, 1−14.
(25) Zhao, Z.; Pu, X.; Xiao, L.; Wang, G.; Su, J.; He, M. Synthesis and properties of high temperature resistant and salt tolerant filtrate reducer N,N-dimethylacrylamide 2-acrylamido-2-methyl-1-propyl dimethyl diallyl ammonium chloride N-vinylpyrrolidone quadripolymer. *J. Polym. Eng.* **2015**, *35*, 627−635.
(26) Abdollahi, M.; Pourmahdi, M.; Nasiri, A. R. Synthesis and characterization of lignosulfonate/acrylamide graft copolymers and their application in environmentally friendly water-based drilling fluid. *J. Pet. Sci. Eng.* **2018**, *171*, 484−494.
(27) Benyounes, K.; Mellak, A.; Benchabane, A. The Effect of Carboxymethylcellulose and Xanthan on the Rheology of Bentonite Suspensions. *Energy Sources A: Recovery Util. Environ. Eff.* **2010**, *32*, 1634−1643.
(28) William, J. K. M.; Ponmani, S.; Samuel, R.; Nagarajan, R.; Sangwai, J. S. Effect of CuO and ZnO nanofluids in xanthan gum on thermal, electrical and high pressure rheology of water-based drilling fluids. *J. Pet. Sci. Eng.* **2014**, *117*, 15−27.
(29) Murtaza, M.; Tariq, Z.; Zhou, X.; Al-Shehri, D.; Mahmoud, M.; Kamal, M. S. Okra as an environment-friendly fluid loss control additive for drilling fluids: Experimental & modeling studies. *J. Pet. Sci. Eng.* **2021**, *204*, No. 108743.
(30) Xiping, M.; Zhongxiang, Z.; Daiyong, H.; Wei, S. Synthesis and performance evaluation of a water-soluble copolymer as high-

performance fluid loss additive for water-based drilling fluid at high temperature. *Russ. J. Appl. Chem.* **2016**, *89*, 1694−1705.
(31) Ghaderi, S.; Ramazani, S. A. A.; Haddadi, S. A. Applications of highly salt and highly temperature resistance terpolymer of acrylamide/styrene/maleic anhydride monomers as a rheological modifier: Rheological and corrosion protection properties studies. *J. Mol. Liq.* **2019**, *294*, No. 111635.
(32) Tan, X.; Duan, L.; Han, W.; Li, Y.; Guo, M. A Zwitterionic Copolymer as Rheology Modifier and Fluid Loss Agents for Water-Based Drilling Fluids. *Polymer* **2021**, *13*, 3120.
(33) Sepehri, S.; Soleyman, R.; Varamesh, A.; Valizadeh, M.; Nasiri, A. Effect of synthetic water-soluble polymers on the properties of the heavy water-based drilling fluid at high pressure-high temperature (HPHT) conditions. *J. Pet. Sci. Eng.* **2018**, *166*, 850−856.
(34) Li, Z.; Pu, X.; Tao, H.; Liu, L.; Su, J. Synthesis and properties of acrylamide 2-acrylamido-2-methypropane sulfonic acid sodium styrene sulfonate N-vinyl pyrrolidone quadripolymer and its reduction of drilling fluid filtration at high temperature and high salinity. *J. Polym. Eng.* **2014**, *34*, 125−131.
(35) Zhu, W.; Zheng, X. Effective Modified Xanthan Gum Fluid Loss Agent for High-Temperature Water-Based Drilling Fluid and the Filtration Control Mechanism. *ACS Omega* **2021**, *6*, 23788−23801.
(36) Davoodi, S.; Ramazani, S. A. A.; Soleimanian, A.; Fellah, J. A. Application of a novel acrylamide copolymer containing highly hydrophobic comonomer as filtration control and rheology modifier additive in water-based drilling mud. *J. Pet. Sci. Eng.* **2019**, *180*, 747−755.
(37) Cao, J.; Meng, L.; Yang, Y.; Zhu, Y.; Wang, X.; Yao, C.; Sun, M.; Zhong, H. Novel Acrylamide/2-Acrylamide-2-methylpropanesulfonic Acid/4-Vinylpyridine Terpolymer as an Anti-calcium Contamination Fluid-Loss Additive for Water-Based Drilling Fluids. *Energy Fuels* **2017**, *31*, 11963−11970.
(38) Liu, F.; Jiang, G.; Peng, S.; He, Y.; Wang, J. Amphoteric Polymer as an Anti-calcium Contamination Fluid-Loss Additive in Water-Based Drilling Fluids. *Energy Fuels* **2016**, *30*, 7221−7228.
(39) Ma, J.; Pang, S.; Zhang, Z.; Xia, B.; An, Y. Experimental Study on the Polymer/Graphene Oxide Composite as a Fluid Loss Agent for Water-Based Drilling Fluids. *ACS Omega* **2021**, *6*, 9750−9763.
(40) Ma, J.; An, Y.; Yu, P. Core-shell structure acrylamide copolymer grafted on nano-silica surface as an anti-calcium and anti-temperature fluid loss agent. *J. Mater. Sci.* **2019**, *54*, 5927−5941.
(41) Ma, J. Y.; Xia, B. R.; Yu, P. Z.; An, Y. X. Comparison of an Emulsion- and Solution-Prepared Acrylamide/AMPS Copolymer for a Fluid Loss Agent in Drilling Fluid. *ACS Omega* **2020**, *5*, 12892−12904.
(42) Nian, Y. J. *Drilling Fluid Technology (Revised Edition)*; China University of Petroleum Press: Shandong, China, 2012.
(43) Li, M.-C.; Wu, Q.; Song, K.; De Hoop, C. F.; Lee, S.; Qing, Y.; Wu, Y. Cellulose Nanocrystals and Polyanionic Cellulose as Additives in Bentonite Water-Based Drilling Fluids: Rheological Modeling and Filtration Mechanisms. *Ind. Eng. Chem. Res.* **2016**, *55*, 133−143.
(44) Alakbari, F. S.; Mohyaldinn, M. E.; Ayoub, M. A.; Muhsan, A. S.; Hassan, A. Apparent and plastic viscosities prediction of water-based drilling fluid using response surface methodology. *Colloids Surf., A* **2021**, *616*, No. 126278.
(45) Luo, Z.; Wang, L.; Pei, J.; Yu, P.; Xia, B. A novel star-shaped copolymer as a rheology modifier in water-based drilling fluids. *J. Pet. Sci. Eng.* **2018**, *168*, 98−106.
(46) Chu, Q.; Lin, L. Synthesis and properties of an improved agent with restricted viscosity and shearing strength in water-based drilling fluid. *J. Pet. Sci. Eng.* **2019**, *173*, 1254−1263.
(47) Alakbari, F, Elkatatny, S, Kamal, M. S., Mahmoud, M. Optimizing the Gel Strength of Water-Based Drilling Fluid Using Clays for Drilling Horizontal and Multi-Lateral Wells. In *SPE Kingdom of Saudi Arabia Annual Technical Symposium and Exhibition*; 2018.
(48) Elkatatny, S.; Kamal, M. S.; Alakbari, F.; Mahmoud, M. Optimizing The Rheological Properties Of Water-Based Drilling Fluid Using Clays And Nanoparticles For Drilling Horizontal And Multi-Lateral Wells. *Appl. Rheol.* **2018**, *28*, 43606.
(49) Shen, X.; Jiang, G.; Li, X.; He, Y.; Yang, L.; Cui, K.; Li, W. Application of carboxylated cellulose nanocrystals as eco-friendly shale inhibitors in water-based drilling fluids. *Colloids Surf. A* **2021**, *627*, No. 127182.
(50) Buijs, W.; Hussein, I. A.; Mahmoud, M.; Onawole, A. T.; Saad, M. A.; Berdiyorov, G. R. Molecular Modeling Study toward Development of H2S-Free Removal of Iron Sulfide Scale from Oil and Gas Wells. *Ind. Eng. Chem. Res.* **2018**, *57*, 10095−10104.
(51) Elkatatny, S. M., Mahmoud, M. A., Nasr-El-Din, H. A. A New technique to Characterize Drilling Fluid Filter Cake. In *SPE European Formation Damage Conference*, 2011.
(52) Elkatatny, S. M., Mahmoud, M. A., Nasr-El-Din, H. A. A New Approach to Determine Filter Cake Properties of Water-Based Drilling Fluids. In *SPE/DGS Saudi Arabia Section Technical Symposium and Exhibition*, 2011.
(53) Mahmoud, M. A., Nasr-El-Din, H. A., De Wolf, C. A. Novel Environmentally Friendly Fluids to Remove Carbonate Minerals from Deep Sandstone Formations. In *SPE European Formation Damage Conference*, 2011.

https://doi.org/10.1021/acsomega.2c01476
ACS Omega 2022, 7, 16141−16151